

# Spherical collapse and cluster number counts in dark energy models disformally coupled to dark matter

Stharporn Sapa<sup>1,\*</sup>, Khamphree Karwan<sup>2,†</sup> and David F. Mota<sup>2‡</sup>

<sup>1</sup>*The Institute for Fundamental Study “The Tah Poe Academia Institute”,*

*Naresuan University, Phitsanulok 65000, Thailand and*

<sup>2</sup>*Institute of Theoretical Astrophysics, University of Oslo, P.O. Box 1029 Blindern, N-0315 Oslo, Norway*

We investigate the effects of a disformal coupling between dark energy and dark matter in the predictions of the spherical collapse and its signatures in galaxy cluster number counts. We find that the disformal coupling has no significant effects on spherical collapse at high redshifts, and in particular during matter domination epoch. However, at lower redshifts, the extrapolated linear density contrast at collapse close to redshift  $z \lesssim 1$  and overdensity at virialization can be strongly suppressed by a disformal coupling between dark energy and dark matter. We also find that the predicted number of clusters per one square degree and redshift is enhanced in dark energy - dark matter models disformally coupled with respect to models with a conformal coupling and models where there is no coupling at all. Increasing the magnitude of the coupling, the number of clusters can be largely enhanced compared with the conformal coupling and uncoupling models at redshift lower than 0.1 in the disformally coupled model.

Keywords: couple dark energy, disformal coupling, spherical collapse, cluster number count

## I. INTRODUCTION

The observational data of Supernova Type Ia (SN Ia) [1–3], cosmic microwave background radiation [4–6], large-scale structure surveys (LSS) [7, 8] indicate that currently the universe is in the phase of accelerating expansion. In order to explain this phenomenon, we can assume that dynamics of the present universe is dominated by dark energy. The observations strongly indicate that the dark energy component corresponds to 70% of the total energy density of the universe. Currently, properties of the dark energy are still unknown. There are many candidates to the dark energy, for instance cosmological constant [9] and scalar fields or quintessence model [10].

Since the nature of dark matter and scalar field candidates to the dark energy are obscure, we can explore properties of dark energy by supposing that dark energy can be coupled with dark matter

\*Electronic address: stharporns57@email.nu.ac.th

†Electronic address: khamphreek@nu.ac.th

‡Electronic address: d.f.mota@astro.uio.no

[11–14]. Although the couplings between dark energy and dark matter are well motivated from theories of particle physics and high energy physics [15–18], it could be more convenient to gain our understanding in general how coupling between dark energy and dark matter can influence the observed universe using phenomenological forms of the coupling which have been variously proposed in literature [19–29]. However, it is also interesting to study the coupling which arises from theoretical motivation. The couplings between dark energy and dark matter can be a consequence of frame transformation of the gravity action. The general transformation of frame which preserves causal structure of the theories is disformal transformation [30–33], and the coupling resulting from this transformation is known as disformal coupling. Influences of the disformal coupling between dark energy and dark matter on evolution of the background universe have been investigated in [34–37], while influences of the couplings on perturbations in the universe, i.e., CMB anisotropies, growth of structures, have been studied in [38–41]

In order to investigate structure formation of matter (ordinary and dark matter), Several authors have used N-body simulations to simulate formation of structure [43–45]. Other easier method for studying the structure formation and the influences of the dark energy to the overdense regions is the spherical collapse model [46–52]. Using spherical collapse model together with Press-Schechter or Sheth-Torman formalism, cluster number counts of halos can be estimated. The cluster number counts can be used to study influence of the dark energy to overdense regions, test and discriminate among the dark energy models. In [53], evolution equations for non-linear perturbations for coupled dark energy models have been derived, and linear as well as non-linear density contrast at virialization for  $\Lambda$ CDM and the coupled dark energy models have been analyzed using spherical collapse. The influences of the coupling between dark energy and dark matter on cluster number counts are investigated in [54, 55]. In [56], the effect of power law  $f(T)$  gravity to spherical collapse and cluster number counts is studied by comparing the results with  $\Lambda$ CDM model. The number density of galaxy clusters is investigated for various form of the potential of dark energy in [57].

In this work, we investigate influences of disformal coupling between dark energy and dark matter on spherical collapse and cluster number counts. The covariant form of the disformal coupling between dark energy and dark matter is presented in section (II). In section (III), the necessary evolution equations for the background universe, linear and non-linear perturbations for dark energy with disformal coupling are shown. Effects of disformal coupling on spherical collapse and cluster number counts are investigated in sections (IV) and (V) respectively. The conclusions are given in section (VI).

## II. DISFORMAL COUPLING BETWEEN DARK ENERGY AND DARK MATTER

Under the disformal transformation the metric tensor is transformed as

$$\bar{g}_{\mu\nu} = C(\phi)g_{\mu\nu} + D(\phi)\phi_{,\mu}\phi_{,\nu}, \quad (1)$$

where subscript  $_{,\mu}$  denotes partial derivative with respect to  $x^\mu$ . Here, we consider the case where the conformal and disformal coefficients  $C$  and  $D$  depend on  $\phi$  only. The inverse of the above metric is

$$\bar{g}^{\mu\nu} = \frac{1}{C^2}(Cg^{\mu\nu} - D\phi'^\mu\phi'^\nu). \quad (2)$$

Let us now suppose that the field  $\phi$  plays a role of dark energy, so that the interaction between dark energy and dark matter can occur when the Lagrangian of dark matter depends on metric  $\bar{g}_{\mu\nu}$  given in Eq. (1). Thus we write the action for gravity in terms of metric  $g_{\mu\nu}$  and write the action for dark matter in terms of  $\bar{g}_{\mu\nu}$  as

$$S = \int d^4x \left\{ \sqrt{-g} \left[ \frac{1}{2}R + P(\phi, X) \right] + \sqrt{-\bar{g}} \mathcal{L}_m(\bar{g}_{\mu\nu}, \psi, \psi_{,\mu}) \right\}, \quad (3)$$

where we have set reduced Planck mass  $m_p = 1/\sqrt{8\pi G} = 1$ ,  $P(\phi, X) \equiv X - V(\phi)$  is the Lagrangian of the scalar field,  $X \equiv -\phi_{,\mu}\phi'^\mu/2$ ,  $V(\phi)$  is the potential of the scalar field and  $\mathcal{L}_m$  is the Lagrangian of dark matter. We will neglect baryon and radiation in our consideration for simplicity, because we will concentrate on the evolution of the universe during matter and dark energy dominated epochs and baryon has no direct coupling with dark energy. Varying this action with respect to  $g_{\alpha\beta}$ , we get

$$G^{\alpha\beta} = T_\phi^{\alpha\beta} + T_m^{\alpha\beta}, \quad (4)$$

where  $G^{\alpha\beta}$  is the Einstein tensor computed from  $g_{\mu\nu}$ , and the energy momentum tensor for scalar field and dark matter are defined in unbarred frame as

$$T_\phi^{\mu\nu} \equiv \frac{2}{\sqrt{-g}} \frac{\delta(\sqrt{-g}P(\phi, X))}{\delta g_{\mu\nu}}, \quad (5)$$

$$T_m^{\mu\nu} \equiv \frac{2}{\sqrt{-\bar{g}}} \frac{\delta(\sqrt{-\bar{g}}\mathcal{L}_m)}{\delta g_{\mu\nu}}. \quad (6)$$

Using these definitions of the energy momentum tensor, Eq. (4) implies  $\nabla_\alpha(T_\phi^{\alpha\beta} + T_m^{\alpha\beta}) = 0$ . However, we see that the energy momentum tensors of dark energy and dark matter do not separately conserve because the Lagrangian of dark matter depends on field  $\phi$ . The energy momentum tensor in the barred frame is related to that in the unbarred frame defined in Eq. (6) as

$$T_m^{\alpha\beta} = \frac{\sqrt{-\bar{g}}}{\sqrt{-g}} \frac{\delta \bar{g}_{\rho\sigma}}{\delta g_{\alpha\beta}} \frac{2}{\sqrt{-\bar{g}}} \frac{\delta(\sqrt{-\bar{g}}\mathcal{L}_m)}{\delta \bar{g}_{\rho\sigma}} = \frac{\sqrt{-\bar{g}}}{\sqrt{-g}} \frac{\delta \bar{g}_{\rho\sigma}}{\delta g_{\alpha\beta}} \bar{T}_m^{\rho\sigma}. \quad (7)$$

Varying the action (3) with respect to  $\phi$ , we obtain

$$\begin{aligned} \phi_{;\alpha}^\alpha - V_{,\phi} &= \nabla_\beta \left( \frac{\sqrt{-\bar{g}}}{\sqrt{-g}} \bar{T}_m^{\alpha\beta} D\phi_{,\alpha} \right) - \frac{1}{2} \frac{\sqrt{-\bar{g}}}{\sqrt{-g}} \bar{T}_m^{\alpha\beta} (C_{,\phi} g_{\alpha\beta} + D_{,\phi} \phi_{,\alpha} \phi_{,\beta}) \\ &\equiv Q, \end{aligned} \quad (8)$$

where  $;$  denotes the covariant derivative and a subscript  $_{,\phi}$  denotes derivative with respect to  $\phi$ . Multiplying the above equation by  $\phi'^{\lambda}$ , we get

$$Q\phi'^{\lambda} = \nabla_{\alpha} T_{\phi}^{\alpha\lambda} = -\nabla_{\alpha} T_m^{\alpha\lambda}. \quad (9)$$

According to [37, 39], the barred quantities in the interaction term  $Q$  can be written in terms of unbarred quantities, so that  $Q$  can be written as

$$Q = \frac{1}{2C^2} \left[ (CD_{,\phi} - 2C_{,\phi}D) \phi_{,\alpha} \phi_{,\beta} T_m^{\alpha\beta} - C \left( C_{,\phi} g_{\alpha\beta} T_m^{\alpha\beta} - 2D(\phi_{;\alpha\beta} T_m^{\alpha\beta} + \phi_{,\alpha} \nabla_{\beta} T_m^{\alpha\beta}) \right) \right]. \quad (10)$$

### III. EVOLUTION EQUATIONS

#### A. Evolution equations in the FLRW universe

Using the FLRW line element,

$$ds^2 = -dt^2 + a^2(t) \delta_{ij} dx^i dx^j, \quad (11)$$

Eq. (4) yields

$$H^2 \equiv \left( \frac{\dot{a}}{a} \right)^2 = \frac{1}{3} \left[ \rho_m + \frac{1}{2}(\dot{\phi})^2 + V(\phi) \right], \quad (12)$$

where a dot denotes derivative with respect to time  $t$  and  $\rho_m$  is the energy density of dark matter. Furthermore, the interaction terms  $Q$  in Eq. (10) becomes

$$Q = \frac{1}{2C^2} \left[ 2(CD_{,\phi} - 2C_{,\phi}D) X \rho_m + C \left( C_{,\phi} \rho_m + 2D(\ddot{\phi} \rho_m + \dot{\phi}(\dot{\rho}_m + 3H\rho_m)) \right) \right], \quad (13)$$

In the above expression, all quantities are evaluated in the background universe, such that  $X \equiv (\dot{\phi})^2/2$ . Inserting this expression for the interaction terms into Eq. (9), we can compute the expression for  $\dot{\rho}_m$ . Substituting the expression for  $\dot{\rho}_m$  back into Eq. (13), and then inserting the result into Eq. (8), we get [37, 39]

$$\begin{aligned} \ddot{\phi} + 3H\dot{\phi} + V_{,\phi} &= \frac{4CC_{,\phi}DX + C^2[2D(3H\dot{\phi} + V_{,\phi}) - (C_{,\phi} + D_{,\phi}X)]}{2C^2[C + D(\rho_m - 2X)]} \rho_m \\ &\equiv -Q_0, \end{aligned} \quad (14)$$

Using the above results, it can be shown that the evolution equations for  $\rho_m$  is

$$\dot{\rho}_m + 3H\rho_m = Q_0\dot{\phi}. \quad (15)$$

### B. Evolution equations for the perturbations on small scales

In order to obtain evolution equations for spherical collapse, we firstly compute the evolution equations for density contrast  $\delta_m \equiv \delta\rho_m/\rho_m$  and velocity perturbation  $v_m^i$  for dark matter on small scales. Supposing that the anisotropic stress disappears, we can write the line element in Newtonian gauge as

$$ds^2 = -(1 + 2\Phi)dt^2 + a^2(1 - 2\Phi)\delta_{ij}dx^i dx^j. \quad (16)$$

On small scales, the Einstein theory of gravity converges to Newtonian limit in which the component  $\mu\nu = 00$  of the perturbed Einstein equation yields [42, 53, 58]

$$\partial_i \partial^i \Phi \equiv \nabla^2 \Phi \simeq \frac{1}{2} \delta\rho_m. \quad (17)$$

Using the approximations  $\nabla^2 \delta\phi \gg \delta\ddot{\phi}, H\delta\dot{\phi}$  for the small scales perturbations, where  $\delta\phi$  is the perturbations in  $\phi$ , Eq. (8) yields

$$\nabla^2 \delta\phi = \delta Q, \quad (18)$$

where  $\delta Q$  is the perturbation in the coupling term  $Q$ . The evolution equations for  $\delta_m$  and  $v_m^i$  can be computed from Eq. (9) by using the energy momentum tensor for dark matter of the form

$$T_m^{\alpha\beta} \equiv (\rho_m + \delta\rho_m) U^\alpha U^\beta, \quad (19)$$

where  $\rho_m$  is the background energy density of dark matter,  $U^\alpha = (1 - \Phi, v_m^i)$  is the four velocity of dark matter and  $v_m^i$  is the 3D comoving velocity of dark matter. Applying the small scales approximation to Eq. (9), the component  $\lambda = 0$  of Eq. (9) on small scales becomes

$$\dot{\delta}_m = -(1 + \delta_m) \partial_i v_m^i - v_m^i \partial_i \delta_m - \widetilde{Q}_0 \dot{\phi} \delta_m + \frac{\delta Q}{\rho_m} \dot{\phi}, \quad (20)$$

where  $\delta_m \equiv \delta\rho_m/\rho_m$  and

$$\widetilde{Q}_0 \equiv \frac{Q_0}{\rho_m} = -\frac{4C_{,\phi}DX - C(C_{,\phi} - 2D(3\dot{\phi}H + V_{,\phi}) + 2D_{,\phi}X)}{2C[C + D(\rho_m - 2X)]}. \quad (21)$$

Similarly, the component  $\lambda = i$  of Eq. (9) on small scales becomes

$$\dot{v}_m^i = -(2H + \widetilde{Q}_0 \dot{\phi}) v_m^i - v_m^j \partial_j v_m^i - (\partial^i \Phi + \widetilde{Q}_0 \partial^i \delta\phi). \quad (22)$$

The perturbations in the interaction term  $\delta Q$  appearing in Eqs. (18) and (20) can be computed by applying the small scales approximation to Eq. (10). On small scales, the dominant contributions in  $\delta Q$  computed from Eq. (10) are

$$\frac{\delta Q}{\rho_m} = \frac{D\dot{\phi}}{C} \left[ \dot{\delta}_m + (1 + \delta_m) \partial_i v_m^i + v_m^i \partial_i \delta_m \right] + \widetilde{Q}_0 \delta_m. \quad (23)$$

Substituting the above equation into Eq. (20), we get

$$\dot{\delta}_m = -(1 + \delta_m) \partial_i v_m^i - v_m^i \partial_i \delta_m. \quad (24)$$

Inserting Eq. (24) into Eq. (23), the term  $\dot{\delta}_m$  can be eliminated and the resulting interaction term is

$$\frac{\delta Q}{\rho_m} = \widetilde{Q}_0 \delta_m. \quad (25)$$

Hence, Eq. (18) becomes

$$\nabla^2 \delta \phi = \widetilde{Q}_0 \delta \rho_m. \quad (26)$$

In order to derive the non-linear evolution equation for  $\delta_m$ , we apply the assumption for top hat density profile [53] to Eqs. (24) and (22), and differentiate these equations with respect to time. After eliminating  $\partial_i \dot{v}_m^i$  from the resulting equations, we get

$$\begin{aligned} \ddot{\delta}_m = & - \left( 2H + \widetilde{Q}_0 \dot{\phi} \right) \dot{\delta}_m + \frac{4}{3} \frac{\dot{\delta}_m^2}{1 + \delta_m} \\ & + (1 + \delta_m) \left( \nabla^2 \Phi + \widetilde{Q}_0 \nabla^2 \delta \phi \right). \end{aligned} \quad (27)$$

To connect Eq. (27) with the evolution of the radius  $r$  of the region which contains dark matter overdensity  $\delta_m$ , the conservation of the number of dark matter particle and the assumption that the mass of dark matter particles in the collapsing region does not differ from that in the background are used. Hence, we have [53]

$$1 + \delta_m = (1 + \delta_{m,in}) \left( \frac{a}{r} \right)^3, \quad (28)$$

where  $\delta_{m,in} \ll 1$  is the initial values of  $\delta_m$  and we have set  $r = a$  initially. The above relation implies that the region with radius  $r$  will collapse if  $\delta_m \rightarrow \infty$ .

#### IV. SPHERICAL COLLAPSE

In order to study spherical collapse, we use

$$C = e^{\lambda_1 \phi}, \quad D = M_d^{-4} e^{\lambda_2 \phi}, \quad V = M_v^4 e^{\lambda_3 \phi}, \quad (29)$$

where  $\lambda_1$ ,  $\lambda_2$  and  $\lambda_3$  are the dimensionless constant parameters, while  $M_d$  and  $M_v$  are the constant parameters with dimension of mass. Using the dimensionless variables

$$x_1^2 \equiv \frac{\dot{\phi}^2}{6H^2}, \quad x_2 \equiv \frac{V}{3H^2}, \quad x_3 \equiv \frac{DH^2}{C}, \quad (30)$$

we can write the evolution equations for the background universe given in section III A in the autonomous form as [36, 37]

$$x_1' = \frac{1}{2} \left( x_1 (3x_1^2 - 3x_2 + 1) - 2(\sqrt{3/2}\lambda_3 x_2 + 2x_1) \right) - \frac{\sqrt{3}}{2\sqrt{2}} (x_1^2 + x_2 - 1) \frac{\lambda_1 (12x_1^2 x_3 - 1) - 6x_3 (\lambda_2 x_1^2 - \sqrt{6}x_1 - \lambda_3 x_2)}{1 - 3x_3 (3x_1^2 + x_2 - 1)}, \quad (31)$$

$$x_2' = x_2 (\sqrt{6}\lambda_3 x_1 + 3x_1^2 - 3x_2 + 3), \quad (32)$$

$$x_3' = -x_3 [3x_1^2 + \sqrt{6}(\lambda_1 - \lambda_2)x_1 - 3x_2 + 3], \quad (33)$$

where a prime denotes derivative with respect to  $N \equiv \ln a$ . The evolution of the background universe is completely described by the above equations. The density parameter of dark matter  $\Omega_m$  is related to the above dimensionless variables through Eq. (12) as

$$1 = x_1^2 + x_2 + \Omega_m. \quad (34)$$

Using the definition in Eq. (30),  $x_3$  can be expressed in terms of  $x_2$  as

$$\begin{aligned} x_3 &= \frac{DM_p^2 H^2}{C} = \frac{M_p^2 H^2}{M_d^4} e^{(\lambda_2 - \lambda_1)\phi/M_p} \\ &= \frac{M_p^2 H_0^2 E^2}{M_d^4} \left( \frac{3M_p^2 H_0^2}{M_v^4} E^2 x_2 \right)^{(\lambda_2 - \lambda_1)/\lambda_3}, \end{aligned} \quad (35)$$

where  $E \equiv H/H_0$  and  $H_0$  is the present value of the Hubble parameter. The reduced Planck mass is restored in the above expression to avoid confusion. From observations, we have  $M_p^2 H_0^2 \simeq 2.7 \times 10^{-47} \text{ GeV}^4 \simeq 27 \text{ meV}^4$ . We choose  $M_d = M_v \simeq 1/0.55 \text{ meV}$  [38]. It follows from Eqs. (31) – (33) and (35) that the evolution equations for  $x_1$ ,  $x_2$  and  $E$  also form a complete set of evolution equations for the background universe. Since the evolution of  $E$  is required to compute cluster number counts in the next section, we solve the evolution equations for  $x_1$ ,  $x_2$  and  $E$  instead of those for  $x_1$ ,  $x_2$  and  $x_3$ . The evolution equation for  $E$  can be computed by differentiating Eq. (12) with respect to  $N$  yielding the result

$$\frac{E'}{E} = \frac{\dot{H}}{H^2} = \frac{3}{2} (x_2 - 1 - x_1^2). \quad (36)$$

In order to numerically solve evolution equations for the background universe, we set initial conditions for  $x_1$  and  $x_2$  such that the density parameter of dark energy  $\Omega_d$  takes value 0.7 at present and equation of state parameter of dark energy  $w_d$  lies within the range  $-1 < w_d < -0.9$ . The initial values for  $E$  is chosen from the requirement that  $E = 1$  at present. We now discuss evolution of the background universe. The coupling term  $\widetilde{Q}_0$  can be written in terms of dimensionless variables as

$$\widetilde{Q}_0 = \frac{\lambda_1 - 6(2\lambda_1 - \lambda_2)x_3x_1^2 - 6\lambda_3x_2x_3 - 6\sqrt{6}x_3x_1}{6(1 - 3x_1^2 - x_2)x_3 + 2}. \quad (37)$$

Inserting Eq. (37) into Eq. (15), we get

$$\dot{\rho}_m + 3H \left( 1 - \sqrt{\frac{2}{3}} \widetilde{Q}_0 x_1 \right) \rho_m = 0. \quad (38)$$

During matter domination, we have  $x_1, x_2 \ll 1$ , so that Eq. (37) becomes

$$\widetilde{Q}_0 = \frac{\lambda_1}{2 + 6x_3}. \quad (39)$$

This suggests that during matter domination, the effects of the conformal coupling quantified by  $\lambda_1$  are suppressed by the amplitude of disformal coefficient quantified by  $x_3$ . For the case where  $0 < \lambda_1, |\lambda_2|, |\lambda_3| \lesssim 1$ , and  $M_d \sim 1\text{meV}$ , the expressions in Eq. (35) gives  $x_3 \sim E^2 \gg 1$  during matter domination. Hence, the disformal coupling can strongly suppress effects of the conformal coupling as well as the magnitude of the coupling during matter domination. In addition to the suppression due to the disformal coupling, the effect of the coupling term in Eq. (38) can be reduced if dark energy slowly evolves, i.e.,  $x_1 \ll 1$ . The magnitude of  $x_1$  is mainly controlled by slope of the potential of dark energy which depends on the parameter  $\lambda_3$ . The other main different feature of the disformal coupling compared with conformal coupling is that the disformal coupling can lead to large magnitude of the coupling between dark energy and dark matter at late time while the coupling is negligible during matter domination. It follows from the Eq. (37) that for  $\lambda_3 < 0$ , the third term in the numerator can enhance the magnitude of the coupling when  $x_2 \sim 0.7$  and  $x_3 \sim 1$  at late time. For the pure conformal coupling case,  $\widetilde{Q}_0 = \lambda_1/2$  during both dark energy and matter domination, so that the evolution of the universe during matter domination may become unphysical if  $\lambda_1 \sim 1$ . During matter domination, if  $\lambda_1 \sim 1$  and  $\rho_d \ll \rho_m$ , where  $\rho_d$  is the energy density of dark energy, the last two terms on the LHS of Eq. (14) will be much smaller than the coupling term on the RHS. Consequently, the dark energy field  $\phi$  will be strongly driven by “external force”  $Q_0$ , and therefore matter dominated epoch will stop quickly and usual acceleration epoch cannot start properly. However, if  $\rho_d$  is not too small compared with  $\rho_m$  during matter domination, the universe can evolve properly although  $\lambda_1 > 1$ . This situation occurs, for example, when dark energy establishes scaling solution during matter domination in the quintessence model with exponential potential (see e.g. [54]). In this case, dark energy in the matter dominated epoch can give a significant contribution to the spherical collapse and cluster number counts [59]. In our consideration, we suppose that dark energy slowly evolves throughout the whole evolution of the universe, so that  $\rho_d \ll \rho_m$  during matter domination.

To check influences of the coupling term  $\widetilde{Q}_0$  on the evolution of  $\rho_m$ , we plot in Figure (1) evolution of  $\bar{\rho}_m/\rho_{m0} \equiv a^3 \rho_m/\rho_{m0}$ . Here,  $\rho_{m0}$  is the present value of  $\rho_m$ . From the plot, we see that  $\rho_m \propto a^{-3}$  at high redshifts. For a fixed  $\rho_{m0}$ ,  $\bar{\rho}_m$  at a given redshift decreases when  $\lambda_1, -\lambda_2$  increase for  $\lambda_3 = -1$ , because  $\widetilde{Q}_0$  increases in this situation. It follows from Eq. (37) that  $\widetilde{Q}_0$  increases when  $\lambda_1$  increases. According to Eq. (35), a negative  $\lambda_2$  can enhance  $x_3$  at late time for negative  $\lambda_3$ , because



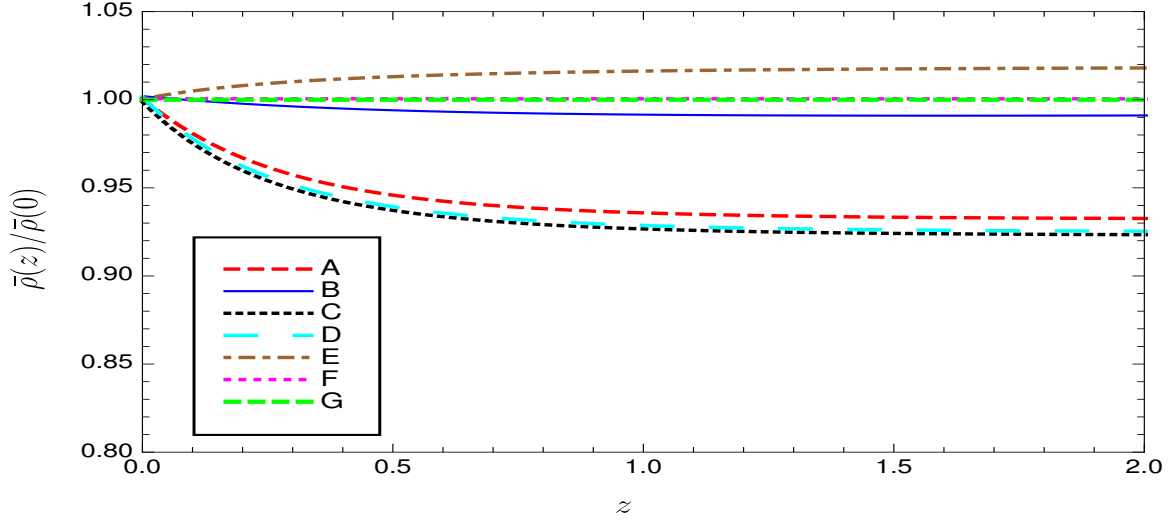


FIG. 1: Plots of  $\bar{\rho}_m/\rho_{m0} \equiv a^3 \rho_m/\rho_{m0}$  as a function of redshift  $z$ . The lines A, B, C, D, E, F represent the case where  $(\lambda_1, \lambda_2, \lambda_3) = (0.1, 0, -1), (0.1, 0, -1), (0.3, -1, -1), (0.1, -1, -1), (0.1, -1, -0.1), (0, 0, -1)$ . The lines A, C, D, E correspond to the disformal coupling cases, while the lines B, F and G respectively corresponds to pure conformal coupling case, uncoupling case and  $\Lambda$ CDM.

$3M_p^2 H_0^2 E^2 x_2 / M_v^4 > 1$ . In the case where  $\lambda_3 = -1$ , the third term in the numerator of Eq. (37) can give a dominant contribution when  $-\lambda_2$  increases due to an enhancement of  $x_3$ . From Eq. (35), we see that the increasing of  $\lambda_3$  from negative value towards zero can enhance  $x_3$  at late time, consequently  $\widetilde{Q}_0$  can become negative due to a large contribution from the fourth term in the numerator of Eq. (37). When  $\widetilde{Q}_0$  becomes negative,  $\rho_m$  will decay faster than  $a^{-3}$  as presented by line E in the Figure (1).

To study how the disformal and conformal coupling influence growth of density perturbations, we insert Eqs. (17) and (26) into Eq. (27), and then write the resulting equation in terms of the dimensionless variables as

$$\begin{aligned} \delta_m'' = & - \left( \frac{1}{2} (1 + 3x_2 - 3x_1^2) + \sqrt{6} \widetilde{Q}_0 x_1 \right) \delta_m' + \frac{4}{3} \frac{(\delta_m')^2}{1 + \delta_m} \\ & + \frac{3}{2} (1 - x_1^2 - x_2) (1 + \delta_m) (1 + 2\widetilde{Q}_0^2) \delta_m. \end{aligned} \quad (40)$$

The linearized version of this equation is

$$\begin{aligned} \delta_m'' = & - \left( \frac{1}{2} (1 + 3x_2 - 3x_1^2) + \sqrt{6} \widetilde{Q}_0 x_1 \right) \delta_m' \\ & + \frac{3}{2} (1 - x_1^2 - x_2) (1 + 2\widetilde{Q}_0^2) \delta_m. \end{aligned} \quad (41)$$

During matter domination,  $\widetilde{Q}_0$  obeys the approximation given in Eq. (39). Hence, for the case where  $x_3 = 0$ , i.e., pure conformal coupling case, Eq. (41) is satisfied by the following growing solution:

$$\delta_m \propto e^{pN}, \quad \text{where} \quad p = -\frac{1}{4} + \frac{1}{4} \sqrt{25 + 12\lambda_1^2}. \quad (42)$$

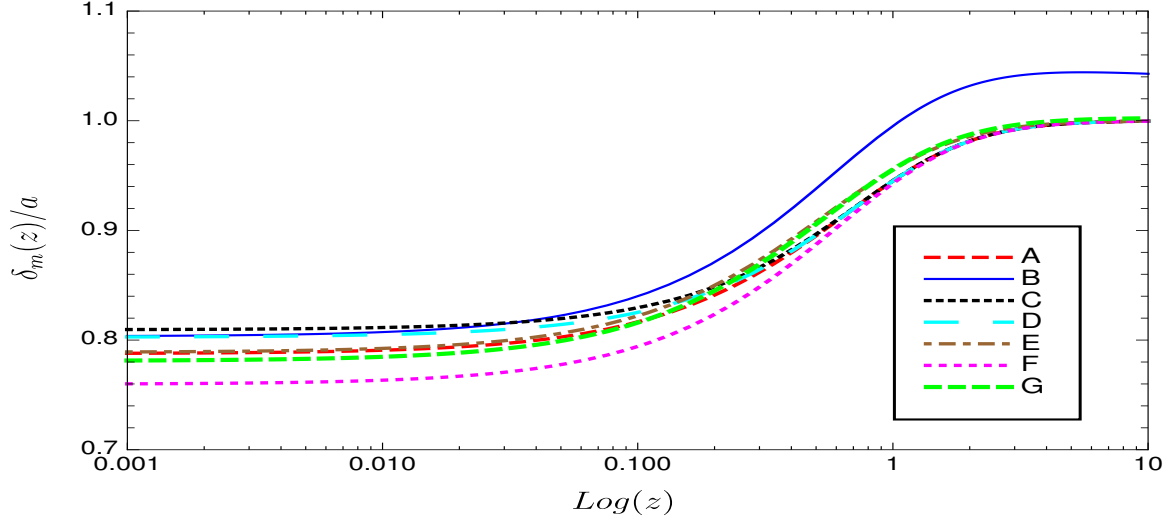


FIG. 2: Plots of  $\delta_m/a$  as a function of redshift  $z$ . The values of  $\lambda_1$ ,  $\lambda_2$  and  $\lambda_3$  for each line are similar to those of the Figure (1). We set  $\delta_m/a = 1$  initially for all cases.

This shows that the conformal coupling can enhance the growth of  $\delta_m$  during matter domination. As discussed above, this enhancement can be disappeared due to disformal coupling which is in agreement with the plots of  $\delta_m/a$  in Figure (2). In the plot, the ratio  $\delta_m/a$  for pure conformal coupling case at a given redshift during matter domination is larger than that for uncoupling case, and this ratio for disformal coupling and uncoupling cases are not significantly different. At late time, the ratio  $\delta_m/a$  for disformal coupling case can decrease slower than or can increase compared with the uncoupling and pure conformal coupling cases which is in agreement with [38]. The decreasing rate of  $\delta_m/a$  for coupling cases at late time depends on  $\widetilde{Q}_0^2$  term which controls “growing rate” of  $\delta_m$  in Eq. (41). In Figure (2), we see that the dependence of decreasing rate of  $\delta_m/a$  on  $\lambda_1$ ,  $\lambda_2$  and  $\lambda_3$  can be understood from the dependence of  $\widetilde{Q}_0$  on these parameters at late time discussed above. We study the spherical collapse in disformal coupling model by compute the extrapolated linear density contrast at collapse  $\delta_c$ . To compute this quantity, we numerically solve Eq. (40) and compute the relation between the collapsing redshift, i.e., redshift at which  $\delta_m \rightarrow \infty$ , and the initial conditions for  $\delta_m$  that lead to the collapse. In our calculation, we fix the initial redshift at  $z = 10^5$  and vary the initial value of  $\delta_m$  within the range  $\delta_m \lesssim 10^{-3}$ . Hence, we can suppose that  $\delta_m$  obeys linear evolution equation given in Eq. (41), and therefore we can set  $\delta'_m = \delta_m$  at initial time. The extrapolated linear density contrast at collapsing redshift  $z$ , denoted by  $\delta_c(z)$ , can be computed by solving Eq. (41) from the initial redshift to the collapsing redshift using the initial value of  $\delta_m$  that lead to the collapse at redshift  $z$ . The plots of  $\delta_c(z)$  are shown in Figure (3). From the plots, we see that increasing the influences from disformal coupling can enhance the decay rate of  $\delta_c$  at late time. This is a consequence of higher growth rate of density perturbation of dark matter for disformal coupling case, i.e., less amount of density perturbations is required for collapsing when growth rate is large, which suggests that

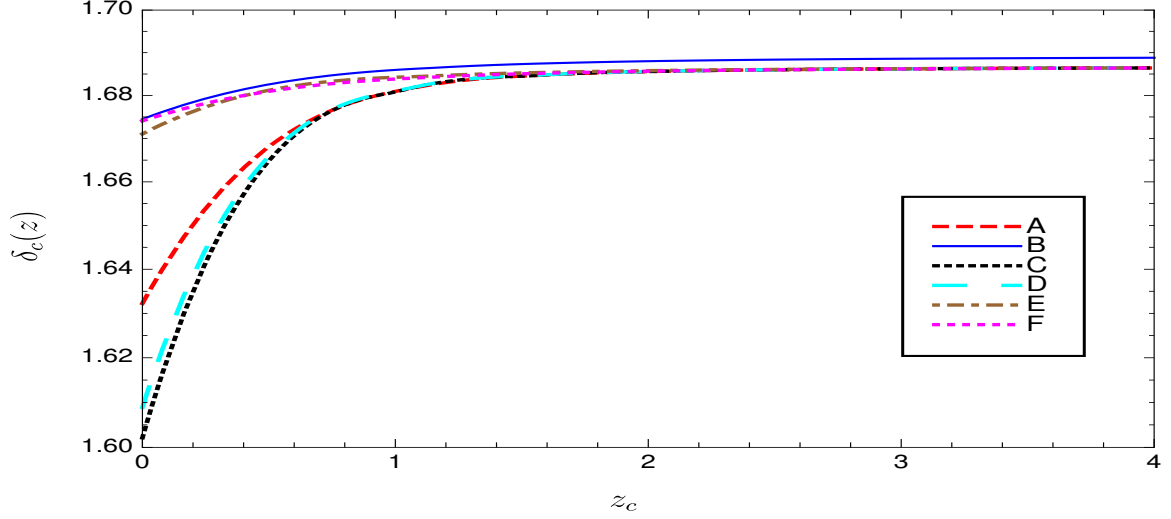


FIG. 3: Plots of  $\delta_c$  as a function of collapsing redshift  $z_c$ . The values of  $\lambda_1$ ,  $\lambda_2$  and  $\lambda_3$  for each line are similar to those of the Figure (1).

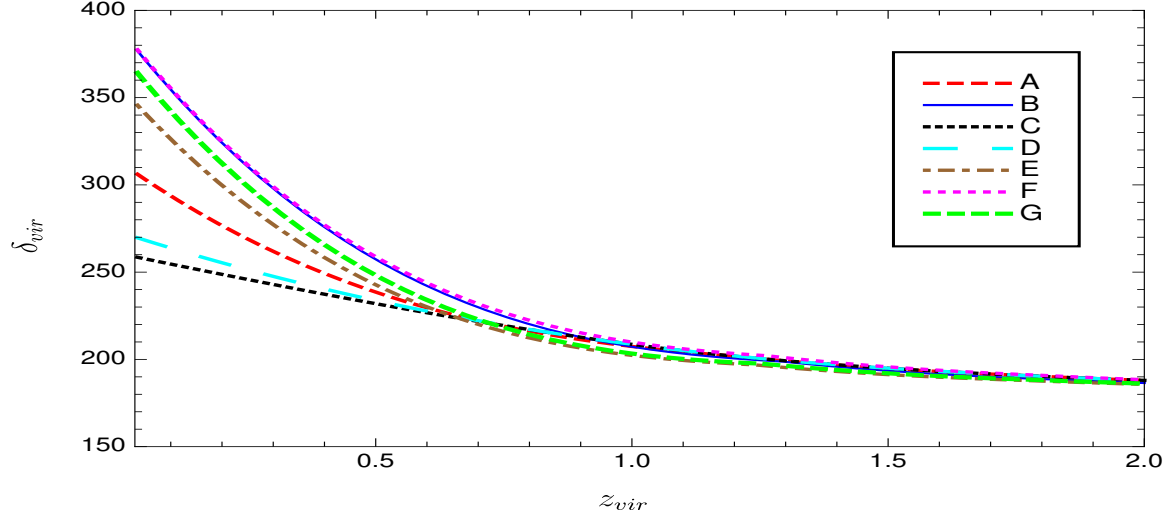


FIG. 4: Plots of  $\delta_{vir}$  as a function of virialized redshift  $z_{vir}$ . The values of  $\lambda_1$ ,  $\lambda_2$  and  $\lambda_3$  for each line are similar to those of the Figure (1).

over dense regions can be efficiently collapsed at late time due to disformal coupling. Using the potential for dark energy derived in [50] with an approximation  $w_d = -1$ , we compute overdensity of dark matter at virialization  $\delta_{vir}$  and plot the results in Figure (4). From the Figure, we see that the disformal coupling can suppress the overdensity at virialization compared with conformal coupling and uncoupling cases. According to our calculation, this is a consequence of low overdensity at turn around in disformal coupling models.

## V. CLUSTER NUMBER COUNTS

In the Press-Schechter (PS) formalism, the mass function which describes the comoving number density of collapsed objects with mass in the range of  $M$  and  $M + dM$  is given by

$$n(M)dM = -\sqrt{\frac{2}{\pi}}\bar{\rho}_m \left(\frac{\delta_c}{\sigma}\right) \frac{d \ln \sigma}{d \ln M} \exp\left(-\frac{\delta_c^2}{2\sigma^2}\right) \frac{dM}{M^2}, \quad (43)$$

where  $\sigma$  is the variance in spheres of radius  $R$  which can be approximately computed from [61]

$$\sigma(R, z) = \sigma_8 \left(\frac{R}{8h^{-1}\text{Mpc}}\right)^{-\gamma(R)} D(z). \quad (44)$$

Here,  $D(z) \equiv \delta_m(z)/\delta(0)$  is the growth factor,  $\delta(0)$  is the linear density contrast of matter perturbation at present and

$$\gamma(R) = (0.3\Omega_m h + 0.2) \left[2.92 + \log_{10} \left(\frac{R}{8h^{-1}\text{Mpc}}\right)\right]. \quad (45)$$

For a better fit with N-body simulation for  $\Lambda$ CDM, an improved form of mass function is proposed using the assumption of ellipsoidal collapse of halo rather than the assumption of spherical halo collapse in PS formalism. This mass function is the Sheth-Tormen (ST) mass function [60],

$$n(M)dM = -0.2709\sqrt{\frac{2}{\pi}}\bar{\rho}_m \frac{d \ln \sigma}{d \ln M} \left(1 + 1.1096 \left(\frac{\delta_c}{\sigma}\right)^{0.6}\right) \exp\left(-\frac{0.707}{2} \left(\frac{\delta_c}{\sigma}\right)^2\right) \frac{dM}{M^2}. \quad (46)$$

A cluster number counts per redshift and square degree with mass  $M \geq M_{\min}$  can be computed from the comoving number density of collapsed objects given in Eq. (43) or (46) by

$$\frac{dN}{dz} = \int_{1\text{deg}^2} d\Omega \frac{dV}{dz d\Omega} \int_{M_{\min}}^{\infty} n(M)dM, \quad (47)$$

where  $dV/dz \equiv d\Omega r(z)^2/(H_0 E(z))$  is the comoving volume element per unit redshift and  $r(z)$  is the comoving distance. In order to understand influences of the disformal coupling on the cluster number counts, we first study how the disformal coupling affects  $dV/dz$  and  $\delta_c/(\sigma D(z))$ . In Figure (5), we plot the evolution of  $(dV/dz)/(dV/dz)_{\text{ES}}$  where  $(dV/dz)_{\text{ES}}$  is the comoving volume element per unit redshift for Einstein-DeSitter model. From the plot, we see that the disformal coupling raises  $dV/dz$  at all redshift compared with the uncoupling and pure conformal coupling cases due to large magnitude of the coupling term  $\widetilde{Q}_0$  at late time. To study effects of disformal coupling on  $\delta_c/(\sigma D(z))$ , we plot  $\delta_c/(\sigma_8 D(z))$  as a function of redshift in Figure (6). For convenience,  $\sigma_8$  for each model with different set of parameters  $\lambda_1, \lambda_2$  and  $\lambda_3$  is set such that the ratio  $\delta_c/(\sigma_8 D(z))$  equals to that for  $\Lambda$ CDM at  $z = 0$ , and  $\sigma_8 = 0.83$  for  $\Lambda$ CDM [4]. For such setting, the value of  $\sigma_8$  for all models, except model E in the plot, lies within the 2- $\sigma$  bound from PLANCK 2015 results [4]. The plots in the Figure (6) show that the ratio  $\delta_c/(\sigma_8 D(z))$  for disformal coupling cases is larger than that for pure conformal coupling and uncoupling cases, which is a consequence of high growth rate of

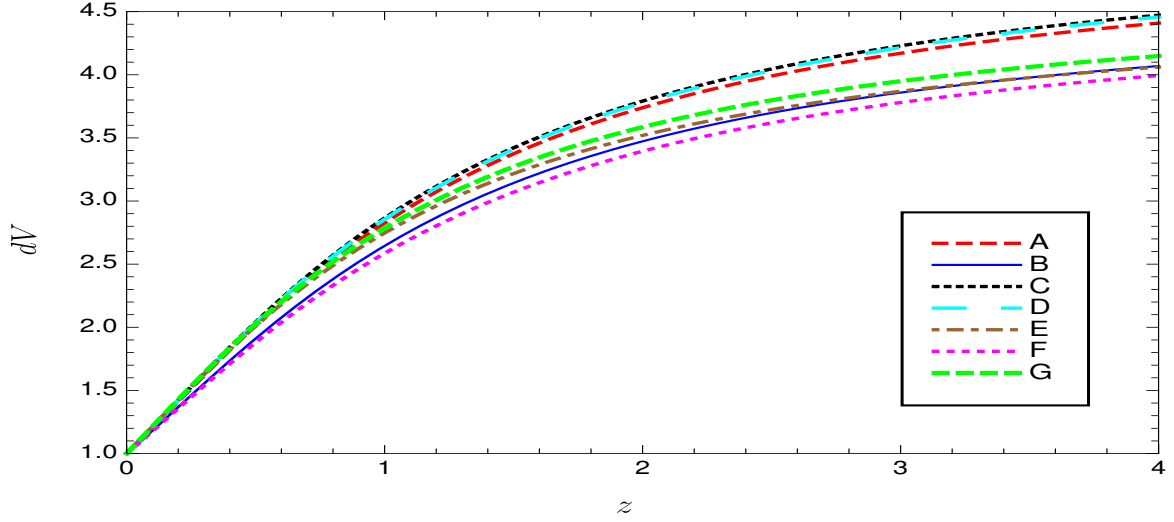


FIG. 5: Plots of  $dV \equiv (dV/dZ)/(dV/dZ)_{\text{ES}}$  as a function of redshift  $z$ . The values of  $\lambda_1$ ,  $\lambda_2$  and  $\lambda_3$  for each line are similar to those of the Figure (1).

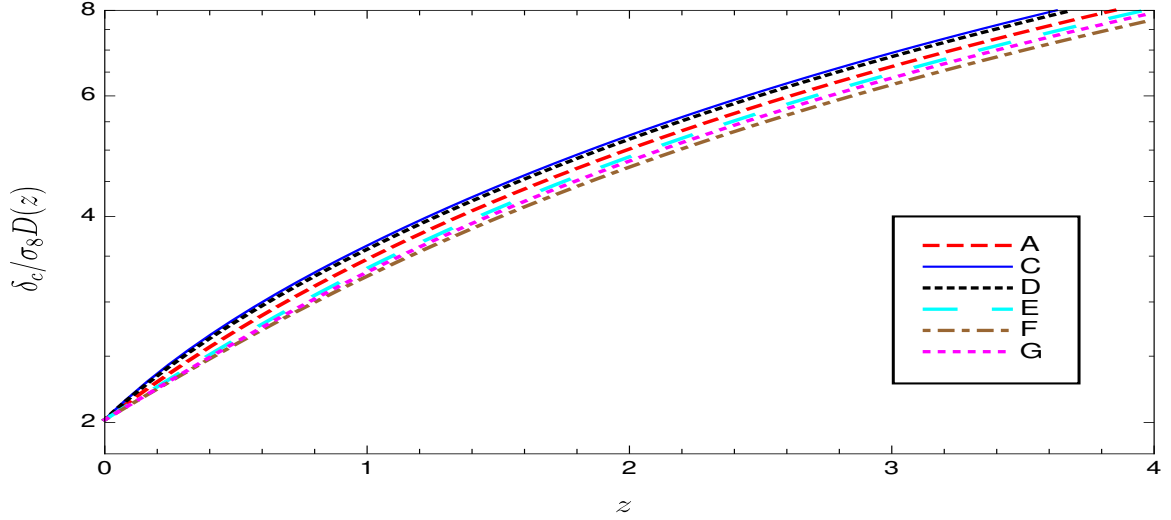


FIG. 6: Plots of  $\delta_c / (\sigma_8 D(z))$  as a function of redshift  $z$ . The values of  $\lambda_1$ ,  $\lambda_2$  and  $\lambda_3$  for each line are similar to those of the Figure (1).

linear density perturbation and low  $\delta_c$  at late time for disformal coupling models, and  $\delta_c / (\sigma_8 D(z))$  is set to unity at  $z = 0$ . We now plot the cluster number counts with  $M \geq M_{\text{min}} = 2 \times 10^{14} M_{\odot} h^{-1}$  if Figure (7). In our study, the predicted cluster number counts from PS and ST mass functions present the same features of conformal and disformal couplings on cluster number counts, so that we plot only the cluster number counts from ST mass function. From the plots, we see that disformal coupling can strongly suppress number of cluster per one square degree and redshift compared with uncoupling case. Mainly, this is a consequence of large  $\delta_c / (\sigma D(z))$  in the disformal coupling models. To investigate effects of disformal coupling on cluster number counts in more detail, In Figure (8), we plot the different ratio  $\Delta_{dN} \equiv (dN/dz)/(dN/dz)_f - 1$  for disformal and conformal coupling cases,

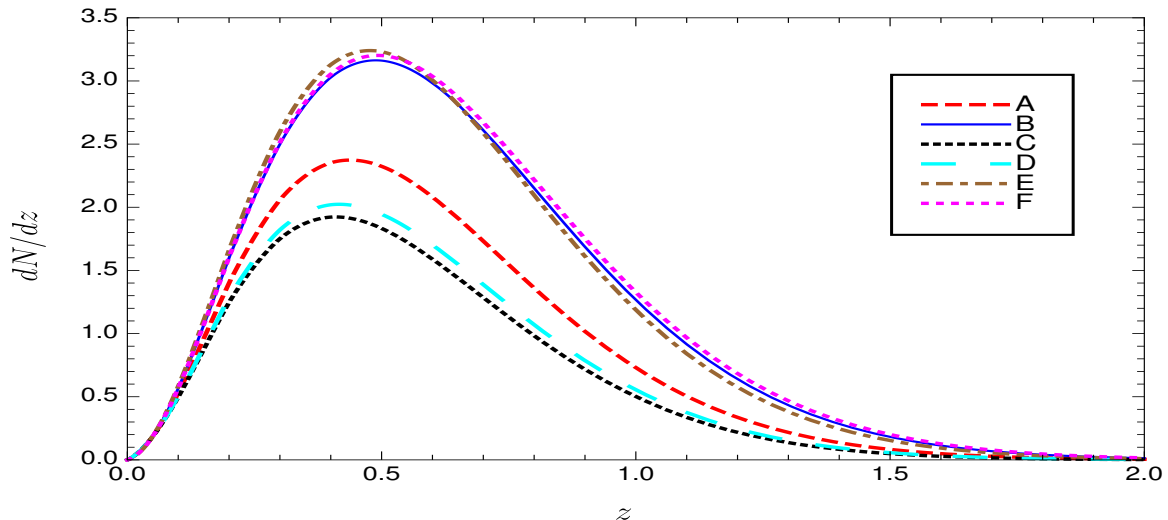


FIG. 7: Plots of  $dN/dz$  with mass  $M \geq M_{\min} = 2 \times 10^{14} M_{\odot} h^{-1}$  as a function of redshift  $z$ . The values of  $\lambda_1$ ,  $\lambda_2$  and  $\lambda_3$  for each line are similar to those of the Figure (1).

where  $(dN/dz)_f$  is  $dN/dz$  for either  $\Lambda$ CDM or uncoupling model. From the plots, we see that at high redshifts the number of cluster per one square degree and redshift for uncoupling dark energy model is larger than that for  $\Lambda$ CDM. The number of cluster is suppressed at high redshift by disformal and conformal couplings. At low redshifts, number of cluster for uncoupling model and  $\Lambda$ CDM models are approximately the same, while the number of cluster can be enlarged compared with uncoupling model by conformal and disformal couplings. The number of cluster can be largely enhanced in disformal models due to a large  $\widetilde{Q}_0$  at late time. The enhancement of the number of cluster at low redshifts is mainly a result from a large  $dV/dz$  in coupling models, so that the choice of  $\sigma_8$  does not significantly affect this enhancement. Moreover, the features of number counts suppression at high redshifts does not significantly depend how the value of  $\sigma_8$  is chosen, in the sense that the conformal and disformal couplings can suppress the cluster number counts and the strong suppression can occur in disformal models.

## VI. CONCLUSION

We investigate influences of disformal coupling between dark energy and dark matter on large scale structure by using the spherical collapse model and the Press-Schechter/Sheth-Torman mass function to estimate cluster number counts. During matter domination, the disformal coupling has no significant effect on the growth rate of density perturbations of dark matter, so that the collapsing properties of an overdense region (radius, virialisation, critical density) is not altered by this type of coupling.

The growth rate of density perturbations of dark matter can be enhanced at late time due to a large

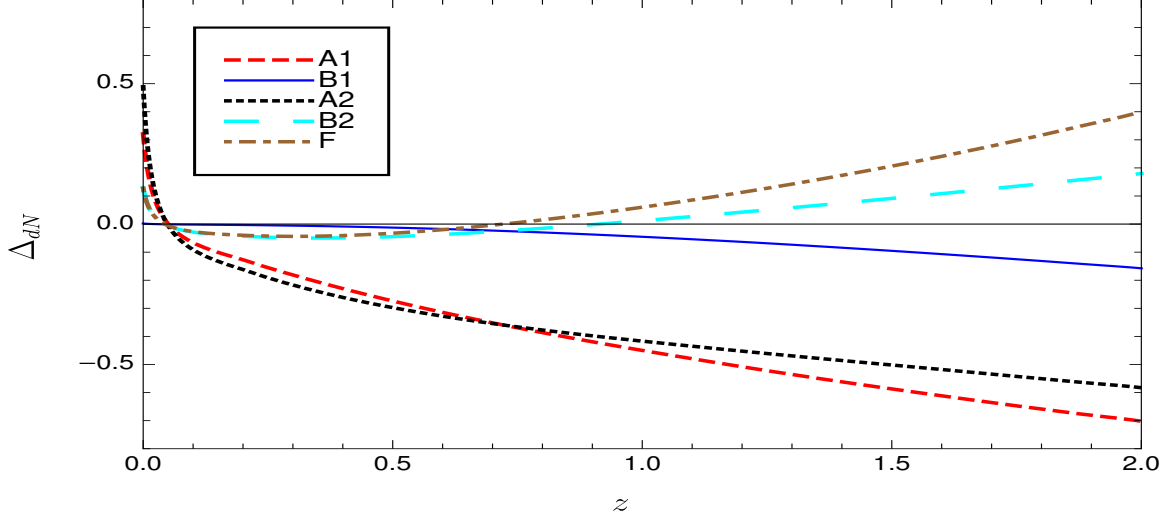


FIG. 8: Plots of different ratio  $\Delta_{dN} \equiv (dN/dz)/(dN/dz)_f - 1$  from  $dN/dz$  presented in the Figure (7). Here, lines  $A_1$  and  $A_2$  represent the different ratio of line A in the Figure (7) with  $\Lambda$ CDM and uncoupling model respectively. Lines  $B_1$  and  $B_2$  represent the different ratio of line B in the Figure (7) with  $\Lambda$ CDM and uncoupling model respectively. Line F corresponds to the different ratio of uncoupling model with  $\Lambda$ CDM.

coupling between dark energy and dark matter in disformally coupled models, as a result, overdense regions can collapse more efficiently at late times, which is suggested by low  $\delta_c$  at low redshifts. Moreover, the overdensity at virialization in the disformal coupling case can be suppressed at low redshifts compared to conformal coupling and uncoupling cases.

Based on the Press-Schechter and Sheth-Torman mass functions, we have found that the predicted number of cluster per one square degree and redshift is strongly suppressed compared with uncoupling model at redshifts larger than 0.5 by disformal coupling due to a large  $\delta_c/(\sigma_8 D(z))$ . Moreover, enhancing the disformal coupling between dark energy and dark matter at late time, the predicted number of cluster can be augmented compared with uncoupling and conformal coupling cases at low redshifts by disformal coupling due to a large comoving volume element per redshift.

### Acknowledgments

KK is supported by Thailand Research Fund (TRF) through grant RSA5780053. DFM thanks the Research Council of Norway for their support and the NOTUR cluster FRAM. This paper is based upon work from COST action CA15117 (CANTATA), supported by COST (European Cooperation in

Science and Technology).

- 
- [1] S. Perlmutter, et al. (Supernova Cosmology Project Collaboration): Nature **391**, 51 (1998), [arXiv:astro-ph/9712212].
  - [2] S. Perlmutter, et al. (Supernova Cosmology Project Collaboration), Astrophys. J., **517**, 565 (1999), [arXiv:astro-ph/9812133].
  - [3] A. Riess, et al. (Supernova Search Team Collaboration): Astron. J., **116**, 1009 (1998), [arXiv:astro-ph/9805201].
  - [4] Planck Collaboration XIII, Planck 2015 results. XIII. Cosmological parameters, A&A, **594**, A 13 (2016), [arXiv:1502.01589 [astro-ph]].
  - [5] E. Komatsu, et al. (WMAP Collaboration): Astrophys. J. Suppl., **192**, 18 (2011), [arXiv:1001.4538 [astro-ph.CO]].
  - [6] D. Larson, et al.: Astrophys. J. Suppl., **192**, 16 (2011), [arXiv:1001.4635v2 [astro-ph.CO]].
  - [7] J. Comparat, T. Delubac, S. Jouvel, et al. 2015, A&A, **592**, A 121 (2016), [arXiv:1509.05045 [astro-ph.CO]].
  - [8] M. Fukugita, T. Ichikawa, J. E. Gunn, et al. , AJ, **111**, 1748 (1996)
  - [9] S. Carroll et al., 1992, Ann. Rev. Astron. Astrophys., **30**, 499 - 542 (1992).
  - [10] B. Ratra and P. Peebles, PRD, **37**, 3406 (1988).
  - [11] L. Amendola, Phys. Rev. D **62**, 043511 (2000), [arXiv:astro-ph/9908023].
  - [12] E. Copeland, M. Sami, S. Tsujikawa, Int. J. Mod. Phys., D **15**: 1753 - 1936, 2006.
  - [13] L. Amendola *et al.*, arXiv:1606.00180 [astro-ph.CO].
  - [14] P. Peebles and B. Ratra, Rev. Mod. Phys., **75**: 559 - 606, 2003.
  - [15] C. Wetterich, Nucl. Phys., B **302**, 668 - 696 (1988).
  - [16] C. Wetterich, Nucl. Phys., B **302**, 645 - 667 (1988).
  - [17] C. Wetterich, Astron. Astrophys., **301**, 321 (1995), [arXiv:hep-th/9408025].
  - [18] G. Farrar and P. Peebles, Astrophys., J **604**, 1 (2004), [arXiv:astro-ph/0307316].
  - [19] P. Peebles and B. Ratra, Astrophys., J **302**, L17 (1988).
  - [20] G. Magnano, G. Miele and V. Pettorino, Mod. Phys. Lett., A **18**, 831 (2003), [arXiv:astro-ph/0212518].
  - [21] C. Boehmer, G. Caldera-Cabral, R. Lakoz and R. Martens, Phys. Rev., D **78**, 023503 (2008), [arXiv:0801.1565 [gr-qc]].
  - [22] G. Caldera-Cabral, R. Martens and L. Urena-Lopez, Phys. Rev., D **063518**, 79 (2009), [arXiv:0812.1827 [gr-qc]].
  - [23] L. Honorez, B. Reid, O. Mena, L. Verde and R. Jimenez, JCAP **1009**, 029 (2010), [arXiv:1006.0877 [astro-ph.CO]].
  - [24] W. Yang and L. Xu, JCAP **1408**, 034 (2014), [arXiv:1401.5177 [astro-ph.CO]].
  - [25] X. Xu, B. Wang, F. Atrio-Barandela, JCAP **1312**, 011 (2013), [arXiv:1308.1475 [astro-ph.CO]].
  - [26] A. Brookfield, C. van de Bruck and L. Hall, Phys. Rev., D **77**, 043006 (200), [arXiv:0709.2297 [astro-ph]].
  - [27] E. Tarrant, C. van de Bruck, E. Copeland and A. Green, Phys. Rev., D **85**, 023503 (2012), [arXiv:1103.10694



[astro-ph.CO]].

- [28] A. Pourtsidou, C. Skordis and E. Copeland, *Phys. Rev., D* **88**, 083505 (2013), [arXiv:1307.0458 [astro-ph.CO]].
- [29] L. Amendola, T. Barreiro and N. Nunes, *Phys. Rev., D* **90**, 083508 (2014), [arXiv:1407.2156 [astro-ph.CO]].
- [30] J. Bekenstein, *Phys. Rev., D* **48**, 3641 (1993), [arXiv:gr-qc/9211917].
- [31] D. Bettoni, S. Liberati, *Phys. Rev., D* **88**, 084020 (2013), [arXiv:1306.6724 [gr-qc]].
- [32] M. Zumalacarregui, T. Koivisto, D. Mota, P. Ruiz-Lapuente, *JCAP* **1005**, 038 (2010), [arXiv:1004.2684 [astro-ph.CO]].
- [33] M. Zumalacarregui and J. Garcia-Bellido, *Phys. Rev., D* **89**, 064046 (2014), [arXiv:1308.4685 [gr-qc]].
- [34] M. Zumalacarregui, T. Koivisto, D. Mota, *Phys. Rev., D* **87**, 083010 (2013), [arXiv:1210.8016 [astro-ph.CO]].
- [35] Jeremy Sakstein and Sarunas Verner, *Phys. Rev., D* **92**, 123005 (2015), [arXiv:1509.05679 [gr-qc]].
- [36] Jeremy Sakstein, *Phys. Rev., D* **91**, 024036 (2015), [arXiv:1409.7296 [astro-ph.CO]].
- [37] K. Karwan and S. Stharporn, *Eur. Phys. J., C* **77**, 352 (2017), [arXiv:1611.05324 [gr-qc]].
- [38] J. Mifsud and C. van de Bruck, *JCAP* **11**, 001 (2017), [arXiv:1707.07667 [astro-ph.CO]].
- [39] C. van de Bruck and J. Morrice, *JCAP* **04**, 036 (2015), [arXiv:1501.03073 [gr-qc]].
- [40] T. Koivisto, D. Mota, M. Zumalacarregui, *Phys. Rev. Lett.* **109**, 241102 (2012), [arXiv:1205.3167 [astro-ph.CO]].
- [41] C. van de Bruck and J. Mifsud, *Phys. Rev. D* **97**, 023506 (2018), [arXiv:1709.04882].
- [42] L. Amendola, *Phys. Rev. D* **69**, 103524 (2004), [arXiv:astro-ph/0311175].
- [43] E. Lokas, P. Bode and Y. Hoffman, *Mon. Not. Roy. Astron. Soc.*, **349**, 595 (2004), [arXiv:astro-ph/0309485].
- [44] Edmund Bertschinger, *Annu. Rev. Astro.*, **36**, 599 - 654 (1998).
- [45] S. Heß, F.-Shu Kitaura and S. Gottloeber, *MNRAS* **435**, 2065 - 2076 (2013), [arXiv:1304.6565 [astro-ph.CO]].
- [46] S. Basilakos, J. C. Bueno Sanchez and L. Perivolaropoulos, *Phys. Rev. D* **80** (2009) 043530
- [47] T. Basse, O. E. Bjaelde and Y. Y. Y. Wong, *JCAP* **1110**, 038 (2011).
- [48] S. Lee and K. W. Ng, *JCAP* **1010**, 028 (2010).
- [49] M. Thorsrud, D. F. Mota and S. Hervik, *JHEP* **1210**, 066 (2012).
- [50] C. Horellou, J. Berger, *Mon. Not. Roy. Astron. Soc.*, **360**, 1393 - 1400 (2005), [arXiv:astro-ph/0504465].
- [51] N. Nunes and D. Mota, *Mon. Not. Roy. Astron. Soc.*, **368**, 751 - 758 (2006), [arXiv:astro-ph/0409481].
- [52] F. Pace, J. Waizmann and M. Bartelmann, *MNRAS* **406**, 1865 - 1874 (2010), [arXiv:1005.0233 [astro-ph.CO]].
- [53] N. Wintergerst and V. Pettorino, *Phys. Rev., D* **82**, 103516 (2010), [arXiv:1005.1278 [astro-ph.CO]].
- [54] M. Manera and D. Mota, *Mon. Not. Roy. Astron. Soc.*, **371**, 1373 (2006), [arXiv:astro-ph/0504519].
- [55] L. R. Abramo, R. C. Batista, L. Liberato and R. Rosenfeld, *JCAP* **0711**, 012 (2007), [arXiv:0707.2882 [astro-ph]].
- [56] M. Malekjani, S. Basilakos and N. Heidari, *MNRAS* **466**, 3488 (2017), [arXiv:1609.01964 [gr-qc]]
- [57] N. Chandrachani Devi, T. Roy Choudhury, Anjan A. Sen, *MNRAS* **432**, 1513 - 1524 (2013), [arXiv:1112.0728 [astro-ph.CO]].
- [58] V. Pettorino and C. Baccigalupi, *Phys. Rev. D* **77**, 103003 (2008), [arXiv:0802.1086 [astro-ph]].
- [59] M. Bartelmann, M. Doran and C. Wetterich, *Astron. Astrophys.*, **454**, 27 - 36 (2006), [arXiv:astro-ph/0507257].

- [60] R. Sheth and G. Tormen, MNRAS **308**, 119 (1999), [arXiv:astro-ph/9901122].
- [61] P. Viana and A. Liddle, MNRAS **303**, 535 (1999).